Mechanism of Lipid Bilayer Disruption by the Human Antimicrobial Peptide, LL-37 †

3 **AUTHORS**, INCLUDING:

Dong-Kuk Lee

74 PUBLICATIONS   **3,341** CITATIONS

SEE PROFILE

Ayyalusamy Ramamoorthy

University of Michigan

336 PUBLICATIONS   **11,746** CITATIONS

SEE PROFILE

Mechanism of Lipid Bilayer Disruption by the Human Antimicrobial Peptide, LL-37[†]

Katherine A. Henzler Wildman, Dong-Kuk Lee, and A. Ramamoorthy*

Department of Chemistry and Biophysics Research Division, University of Michigan, Ann Arbor, Michigan 48109

Received December 12, 2002

ABSTRACT: LL-37 is an amphipathic, α-helical, antimicrobial peptide. ^{15}N chemical shift and ^{15}N dipolar−shift spectroscopy of site-specifically labeled LL-37 in oriented lipid bilayers indicate that the amphipathic helix is oriented parallel to the surface of the bilayer. This surface orientation is maintained in both anionic and zwitterionic bilayers and at different temperatures and peptide concentrations, ruling out a barrel-stave mechanism for bilayer disruption by LL-37. In contrast, electrostatic factors, the type of lipid, and the presence of cholesterol do affect the extent to which LL-37 perturbs the lipids in the bilayer as observed with ^{31}P NMR. The ^{31}P spectra also show that micelles or other small, rapidly tumbling membrane fragments are not formed in the presence of LL-37, excluding a detergent-like mechanism. LL-37 does increase the lamellar to inverted hexagonal phase transition temperature of both PE model lipid systems and *Escherichia coli* lipids, demonstrating that it induces positive curvature strain in these environments. These results support a toroidal pore mechanism of lipid bilayer disruption by LL-37.

The increasing prevalence of antibiotic resistance necessitates the development of new ways to combat bacterial infection. Antimicrobial peptides represent a promising means for meeting this challenge (*1*). Unlike current antibiotics, which interact strongly with specific target molecules, usually proteins, most antimicrobial peptides act by a nonspecific mechanism and often induce cell death by disrupting the plasma membrane (*1*). Selective antimicrobial peptides distinguish between eukaryotic cells and bacterial cells based on variations in the composition of the cell membrane (*1*). In the case of eukaryotic cells, the primary membrane features are the presence of cholesterol, predominance of PC[1] lipids, and a nearly neutral outer membrane. Bacterial cells lack cholesterol, have PE as their most common zwitterionic lipid, and have 20−25% negatively charged lipids in their outer membranes. Since the majority of α-helical, amphipathic, antimicrobial peptides are positively charged at physiological pH, the prevailing theory is that selectivity results from electrostatic attraction of the cationic peptide to the anionic bacterial membranes (*2*). While some highly selective peptides such as magainins and cecropins fit this model, electrostatics cannot be the only source of selectivity because other highly amphipathic cationic peptides, including melittin and mastoparan, are nonselective toxins (*3*). Thus, other aspects of membrane composition and additional peptide properties must also be important in determining selectivity. Extensive mutational and calorimetric studies of magainins by Dathe et. al. have shown that although electrostatic attraction increases the concentration of peptide at the membrane surface, disruption of the membrane depends on hydrophobic interactions of the peptide and membrane regardless of whether the membrane is neutral or anionic (*3*, *4*). Therefore, more subtle hydrophobic properties of the peptide, including its hydrophobic moment and angle subtended by the hydrophobic face of the helix, are crucial in determining the extent of peptide insertion and disruption of membrane integrity. Understanding the mechanism of membrane disruption by a variety of peptides in many different types of membranes is necessary to elucidate the various factors determining the activity of a peptide in a particular membrane environment and to design therapeutic peptides with the desired potency and selectivity.

There is little homology among antimicrobial peptides except for their amphipathic topology, and active antimicrobial peptides can have any type of secondary structure (*1*). Slight differences in charge, hydrophobicity, and relative size of hydrophobic and hydrophilic domains lead to very different behavior in membranes in a manner that is not well understood (*3*). Seemingly similar peptides exhibit a wide range of orientations, regularity and size of holes in the bilayer, and peptide effect on lipid flip-flop, headgroup tilt, curvature strain, and acyl chain disordering. Three primary mechanisms have been proposed to explain this variation in behavior as reviewed in refs *1*, *5−9*). Some peptides, such as alamethicin, form well-defined barrel-stave pores with the

---

* To whom correspondence should be addressed: Telephone: (734) 647-6572. Fax: (734) 764-3323. E-mail: ramamoor@umich.edu.

[1] CD, circular dichroism; CF, cystic fibrosis; CP, cross polarization; CSA, chemical shift anisotropy; DiPoPE, 1,2-dipalmitoleoyl-*sn*-glycero-3-phosphatidylethanolamine; DMPC, 1,2-dimyristoyl-*sn*-glycero-3-phosphatidylcholine; DMPG, 1,2-dimyristoyl-*sn*-glycero-3-phosphatidylglycerol; DSC, differential scanning calorimetry; LL-37-*U*, unlabeled LL-37; LL-37-*L*, ^{13}C$_\alpha$-Ala$_{13}$-^{15}N-Val$_{21}$-^{13}C′-Leu$_{31}$-LL-37; MAS, magic angle spinning; MIC, minimum inhibitory concentration; MLV, multilamellar vesicle; PC, phosphatidylcholine; PG, phosphatidylglycerol; PS, phosphatidylserine; POPC, 1-palmitoyl-2-oleoyl-*sn*-glycero-3-phosphatidylcholine; POPE, 1-palmitoyl-2-oleoyl-*sn*-glycero-3-phosphatidylethanolamine; POPG, 1-palmitoyl-2-oleoyl-*sn*-glycero-3-phosphatidylglycerol; S/N, signal-to-noise ratio; SUV, small unilamellar vesicle; TFA trifluoroacetic acid.

peptide inserted into the bilayer and its hydrophilic face lining the water-filled pore (10−12). Other peptides have only been observed to lie on the surface of the membrane, or insert very transiently, and are considered to operate by toroidal pore or carpet mechanisms. The toroidal pore mechanism was developed based on the behavior of magainins and involves the induction of curvature strain in the bilayer by the peptide, leading to the formation of transient, toroidal lipid-peptide pores when there is a high local concentration of peptide (13−15). An alternative mechanism for surface-oriented peptides is the carpet model, which is characterized by general disruption of the bilayer in a detergent-like manner, eventually leading to the formation of micelles at high peptide concentrations (8, 16). In this study, we report the mechanism of lipid bilayer disruption by the human antimicrobial peptide LL-37.

LL-37 is a 4.5-kDa human, cationic, amphipathic, α-helical, antimicrobial peptide with the sequence LLGDFFRK-SKEKIGKEFKRIVQRIKDFLRNLVPRTES (17). Although highly charged (16 charged residues, net +6 at neutral pH), it is not as selective as some α-helical, amphipathic, antimicrobial peptides, with MICs ranging from 1 to 10 μM for a variety of gram positive and gram negative bacteria, and eukaryotic cytotoxicity occurring at 13−25 μM in vitro (18−21). The antimicrobial activity of LL-37 has been confirmed in vivo as well (22). A highly selective peptide, such as magainin (MIC 5 μg/mL, no hemolysis up to 150 μg/mL) (23), has a larger difference between the concentration required to kill bacterial and eukaryotic cells. However, LL-37 is not insensitive to membrane composition. Some bacterial strains that colonize the lungs have developed resistance to LL-37 by adding choline headgroups to lipopolysaccharide or other nonphospholipids in their outer membrane (24). This suggests that although choline headgroups do not prevent membrane disruption by LL-37, since it lyses eukaryotic cells with choline-rich membranes, the headgroups may modulate LL-37−membrane interactions either directly or through their effect on other properties of the lipid bilayer to which LL-37 is sensitive. LL-37 aggregation is also sensitive to bilayer composition, with a higher aggregation state in zwitterionic PC bilayers than in negatively charged PC/PS bilayers (25).

LL-37 has a mainly α-helical secondary structure and is aggregated in aqueous solutions at physiological pH and ionic strength. Its conformation is sensitive to salt concentration, with LL-37 assuming a random coil configuration in pure water and becoming α-helical in the presence of millimolar anion concentrations (18). The helical conformation of LL-37 is stable over a wide range of buffer conditions, including high salt, and is also the same in the presence of lipids (19, 25, 26). Sequence analysis reveals that LL-37 can form an amphipathic α-helix from residues 11−32, which matches the percent helicity determined from CD data (19, 27). The formation of helical structure also correlates with LL-37 aggregation and activity (18, 25), which occurs at micromolar peptide concentrations in the presence of anions. This helical, aggregated form of LL-37 in solution is very different from other amphipathic, α-helical, antimicrobial peptides that are monomeric and unstructured in aqueous solution and only become α-helical upon association with a membrane. Calorimetric studies of magainin derivatives have shown that this conformational change from random coil to α-helix

provides a large portion of the thermodynamic driving force for membrane binding and insertion (28). In contrast, LL-37−membrane interactions must have a different energetic basis since it is helical in both physiological buffer conditions and upon association with the membrane and does not undergo a conformational change.

This unique stability of LL-37 structure under a variety of conditions, including high salt concentrations, could be useful in treating cystic fibrosis (CF). Four times the normal level of LL-37 expression restored normal bacterial killing in a rat bronchial xenograft model of CF, suggesting that LL-37 may be an effective addition to CF treatment (29). CF is characterized by chronic lung infections that cannot be cured by antibiotics, usually causing death by the mid 30s. It is caused by mutation of the CF transmembrane conductance regulator chloride channel, and this defect leads to abnormal conditions at the surface of the lung epithelia, in particular, elevated salt concentrations that inhibit many of the usual antibacterial defenses in the lung (26, 29).

To better understand the mechanism of LL-37 activity, this work investigates the mechanism of lipid bilayer disruption by LL-37 using solid-state NMR and differential scanning calorimetry (DSC). The extent of the amphipathic α-helical region was confirmed using ^{13}C solid-state NMR and the orientation of the helix parallel to the surface of lipid bilayers was determined using ^{15}N solid-state NMR of site-specifically labeled LL-37. ^{31}P NMR reveals the perturbation of the lipid headgroups when LL-37 is incorporated into lipid bilayers, but shows that small bilayer fragments or micelles are not formed. A combination of ^{31}P NMR and differential scanning calorimetry shows that LL-37 induces positive curvature in the membrane. Together, these results support a toroidal pore model of bilayer disruption, rather than a barrel-stave or detergent-like micellization mechanism.

DMPC was chosen as the initial lipid system for detailed characterization of the interaction of LL-37 with lipid bilayers because it is simple and well characterized. As a zwitterionic lipid with symmetric, saturated acyl chains, the lipid properties are well-known (30), aiding in interpretation of the data. In addition, the interaction of LL-37 with lipids containing choline headgroups is of interest because of the possible role of phosphorylcholine in bacterial resistance to LL-37 (24), although the presence of phosphatidylcholine headgroups on phospholipids does not prevent membrane disruption by LL-37. DMPC has also been widely used in other studies of peptides that interact with lipid bilayers, enabling comparison of the results of this work with studies of other antimicrobial peptides and membrane-perturbing molecules (31−39), thus allowing insight into the mechanism of membrane disruption and the similarities and differences exhibited by the various cationic, amphipathic, α-helical peptides. It also provides a good baseline for comparison when the bilayer composition is varied. The results presented here also examine the effects of headgroup charge, acyl chain unsaturation, and the presence of cholesterol in the membrane on the interaction of LL-37 with lipid bilayers. Although LL-37 is a highly charged cationic peptide, it is still hydrophobic enough to penetrate into the core of the bilayer, and is not highly selective. The interaction of LL-37 with lipid bilayers varies with the membrane composition and aqueous environment (the ionic strength, pH, etc. of the buffer or water hydrating the bilayers), thus its behavior in a variety of lipid types is

necessary in order to understand its function. Understanding the method of disruption in several types of membrane is also important for discerning the reasons for its limited selectivity and ability to kill eukaryotic cells, important considerations for the future development of amphipathic cationic antimicrobial peptides as therapeutic agents.

EXPERIMENTAL PROCEDURES

Materials. Peptide synthesis and cleavage reagents were purchased from Applied Biosystems (Foster City, CA) and Aldrich (Milwaukee, WI), respectively. Fmoc-protected amino acids were from Advanced ChemTech (Louisville, KY), and isotopically labeled Fmoc-amino acids were from Cambridge Isotope Labs (Cambridge, MA). Lipids and *Escherichia coli* total lipid extract were purchased from Avanti Polar Lipids, Inc. (Alabaster, AL). Chloroform and methanol were from Aldrich (Milwaukee, WI) and all other reagents were from Fisher (Pittsburgh, PA).

Peptide Synthesis. LL-37 (LLGDFFRKSKEKIGKEFKR-IVQRIKDFLRNLVPRTES) was synthesized on an ABI-431A (Applied Biosystems, Foster City, CA) peptide synthesizer using FastMoc chemistry with double coupling and double deprotection. LL-37-*U* refers to this peptide, which does not contain any isotopic labels. Site-specifically labeled LL-37 (LL-37-*L*) was also synthesized, incorporating three labels: ^{15}N at Val_{21}, $^{13}C=O$ at Leu_{31}, and $^{13}C_\alpha$-Ala in place of Ile_{13}. Alanine was substituted for isoleucine at residue 13 due to the very limited availability of $^{13}C_\alpha$- and $^{13}C=O$-labeled Fmoc amino acids as required for the synthesis. Incorporating the $^{13}C=O$ label in the leucine near the C-terminus of the helix and replacing Ile_{13} with $^{13}C_\alpha$-Ala was thus the most conservative way of incorporating three well-resolved labels in a single synthetic peptide, reducing the time and cost required for synthesis. Cleavage from the Ser(*t*-Bu)-Wang resin (Peptides International) to produce a free carboxylate at the C-terminus and deprotection were accomplished using TFA and scavengers. The peptides were purified by HPLC, washed with 1% acetic acid to remove residual TFA, and lyophilized from water at a concentration of about 1 mg/mL. Characterization of the peptides by mass spectrometry and analytical HPLC indicated that both had the correct molecular weight and were >96% pure.

Sample Preparation. LL-37-*L* was used in all the samples prepared for ^{13}C and ^{15}N NMR experiments. Samples for ^{31}P NMR, DSC, and CD experiments used LL-37-*U*. All of the peptide concentrations are reported as peptide/lipid mole ratio, or are given in mole% of peptide relative to the total moles of peptide plus lipid.

Multilamellar vesicle (MLV) samples were prepared by mixing the desired amounts of peptide and lipid in 2:1 CHCl$_3$/MeOH. The peptide/lipid samples were dried under a stream of nitrogen and then under vacuum overnight to completely remove any residual solvent. Tris buffer (10 mM Tris, 100 mM NaCl, 2 mM EDTA, pH 7.4) was added to the DSC MLV samples to produce a final lipid concentration of 0.10 mg/mL DiPOPE. The NMR MLV samples were hydrated with 50 weight % water. The samples were vortexed for 2 min above the lipid phase transition temperature and freeze−thawed using liquid nitrogen several times to ensure a uniform mixture of lipid and peptide. All MLV samples were stored at −20 °C prior to use.

Small unilamellar vesicles (SUVs) for CD spectroscopy were prepared by mixing the lipids in chloroform, drying off the solvent under a stream of nitrogen and then under vacuum, hydrating with an appropriate amount of water or phosphate buffer (20 mM phosphate, pH 7.2) to create a 3 mM lipid stock, and sonicating until the solution was optically clear, ≈5 min. Peptide stock solutions (200 μM) were prepared by dissolving dry peptide in water or phosphate buffer.

Oriented samples for solid-state ^{31}P and ^{15}N NMR were prepared using a slight modification of a procedure developed in our lab utilizing naphthalene to create a more porous peptide/lipid film which aids in hydration (*40*). Peptide and lipids were mixed in 2:1 CHCl$_3$/MeOH using 2 mg of lipid for ^{31}P samples and 100 mg of lipid for ^{15}N samples. The lipid/peptide mixture was dried under nitrogen and resuspended in 2:1 CHCl$_3$/MeOH with a 5:1 mole ratio of naphthalene to lipid/peptide. This solution was spread on 1 (^{31}P) or 25 (^{15}N) thin glass plates (11 mm × 22 mm × 50 μm, Paul Marienfield, GmbH, Bad Mergentheim, Germany), allowed to air-dry, and then vacuum-dried overnight. The plates were then indirectly hydrated for 3−5 days in a 37 °C hydration chamber at 93% relative humidity, which is maintained above a saturated ammonium phosphate solution. Following indirect hydration, 30 mol of H$_2$O per mole lipid/peptide was added and the plates were stacked, covered with a top plate, and sealed in plastic using a bag sealer (Plastic Bagmart, Marietta, GA) to prevent dehydration. The samples were then allowed to equilibrate an additional 3−6 days at 5−10 °C above the main phase transition temperature of the lipids before being used for NMR experiments. An equal volume of tris buffer was used to directly hydrate some samples instead of water, and this is noted in the figure captions and text.

CD. Peptide and lipid SUV stocks were mixed in a 5-mm cuvette with additional buffer or water to make each CD sample. The cuvette containing the sample was then equilibrated to 35 °C in the CD spectrometer (AVIV, Lakewood, NJ) and three scans of the CD spectrum were taken and averaged. Baseline spectra of buffer with the same concentration of lipid SUVs were subtracted to isolate the peptide signal.

DSC. All buffers and samples were degassed under vacuum for 15 min before being loaded into the Nano-DSC II calorimeter (Calorimetry Sciences Corp., Provo, UT). The scan rate was 0.25 °C/min over the temperature range 15−65 °C with 10 min equilibration between scans. Initial heating and cooling scans of buffer alone were run before each sample to provide a baseline. The sample was loaded below the lamellar to inverted hexagonal phase transition temperature (T_H) and three additional heating and cooling scans were run to ensure that the first scan was not anomalous. DSC experiments were run with samples containing P/L mole ratios of 1:5000, 1:1000, 1:500, and 1:100 in DiPoPE. The raw data were converted to molar heat capacity using the CPCalc program provided with the calorimeter and the lipid concentration and molecular weight of each sample along with a partial specific volume of 0.988 mL/g (*30*).

^{31}P, ^{13}C, and ^{15}N NMR. ^{31}P, ^{13}C, and ^{15}N NMR spectra were acquired using a Varian/Chemagnetics 400 MHz spectrometer with ^1H, ^{31}P, ^{13}C, and ^{15}N frequencies of

400.139, 161.978, 100.618, and 40.551 MHz, respectively. Home-built, double-resonance, flat-coil probes were used for the mechanically aligned samples with a coil just large enough to hold the samples. The flat coils were made of 2-mm wide flat copper wire with 1-mm spacing between turns and 4−6 turns per coil. The bilayers were oriented with the bilayer normal parallel to the magnetic field unless otherwise noted. A commercial Varian/Chemagnetics double resonance MAS probe with a 5-mm zirconia MAS rotor was used to acquire the static and MAS spectra of the dry peptide and ^{31}P spectra of unoriented MLV samples. Spectra were processed using Chemagnetics Spinsight software on a Sun Sparc workstation and Igor Pro 3.14 (Wavemetrics, Lake Oswego, OR) on an iMac.

^{31}P chemical shift spectra of mechanically aligned bilayer samples were obtained using a chemical shift echo sequence, 90°-τ-180°-τ-acq, with $\tau = 100$ μs and 25 kHz ^{1}H decoupling. Typical ^{31}P $\pi/2$ pulse lengths were 3−3.5 μs and the spectral width was 50 kHz. An average of 2000 transients were averaged with a recycle delay of 3 s. The spectra of oriented samples were referenced with respect to 85% H$_3$-PO$_4$ between glass plates (0 ppm), since this differs from the chemical shift of a cylindrical capillary sample of 85% H$_3$PO$_4$ by several ppm. The FID was processed beginning at the top of the echo with 80 Hz exponential broadening, zero filled to 4096 points and Fourier transformed. Samples for each ^{31}P experiment were prepared several times independently, and the spectra were compared to confirm the results.

All the ^{15}N spectra of labeled LL-37 in lipid bilayers were acquired using cross-polarization with a ^{1}H $\pi/2$ pulse length of 3−3.5 μs, 45−55 kHz CP power, and ^{1}H decoupling of 65−75 kHz during acquisition. The recycle delay was 5 s and the spectral width was 50 kHz. The ^{15}N chemical shift spectra of 2% LL-37-*L* in oriented DMPC bilayers were acquired using a 5-ms ramp CP with a 10 kHz ramp on the ^{1}H channel. The number of scans required for adequate S/N varied with temperature; $\approx$15 000 scans were acquired at 25 and 35 °C, while $\approx$70 000 scans were acquired at 50 °C for the 2% LL-37-*L* in DMPC samples. The ^{15}N chemical shift powder pattern of 2% LL-37-*L* in DMPC MLVs was acquired with the same parameters except that a 2-ms nonramped CP was used. The 1-D ^{15}N dipolar-shift spectra (*41*) were acquired using the same parameters as the chemical shift spectra, but with a 2-ms nonramped CP and the ^{1}H decoupling frequency was offset to create an effective field at the magic angle (*41*). All the spectra were processed with 120 Hz exponential broadening and referenced to powder (^{15}NH$_4$)$_2$SO$_4$ at 24.1 ppm relative to liquid NH$_3$.

^{13}C and ^{15}N static and MAS spectra of dry powder peptide samples were obtained with a MAS speed of 5 kHz and all other parameters the same as for the peptide in MLV sample. ^{15}N spectra were referenced as above, and the ^{13}C spectra were referenced with respect to TMS via adamantane at 29.5 and 38.6 ppm.

The principal values of the ^{15}N-Val$_{21}$ chemical shift tensor were determined from the best fitting simulation of the powder spectrum. The spectrum was simulated using Igor Pro 3.14 (Wavemetrics, Lake Oswego, OR) and

$$\delta_{CS} = \sigma_{11} \cos^2\phi \sin^2\theta + \sigma_{22} \sin^2\phi \sin^2\theta + \sigma_{33} \cos^2\theta \quad (1)$$

where θ and ϕ are as defined in Figure 3F. The principal values are reported using the convention that $\sigma_{33} \geq \sigma_{22} \geq \sigma_{11}$. The oriented chemical shift spectra were simulated using the principal values of the chemical shift tensor obtained from the powder pattern to determine the angles θ and ϕ. The 1-D dipolar-shift powder spectrum was simulated to determine the orientation of the principal axes of the ^{15}N-Val$_{21}$ chemical shift tensor with respect to the ^{15}N−^{1}H bond. Both the ^{15}N chemical shift and scaled ^{15}N−^{1}H dipolar coupling contribute to the dipolar-shift spectrum as described by the equations for δ_{CS} in ref 2 for the chemical shift and ω_{NH} for the dipolar coupling:

$$\omega_{NH} = 0.58(D_{NH}/2)[1 - 3\{\sin\theta \sin\beta \cos(\phi - \alpha) + \cos\theta \cos\beta\}^2] \quad (2)$$

where $D_{NH} = \mu_o h \gamma_N \gamma_H / 8\pi^2 r_{NH}^3$, and β, α, θ, and ϕ are as defined in Figure 3F. Gaussian line broadening was used in all the simulations. The best fitting spectra were determined by comparing both the frequency and intensities of the features in the spectra. Further details on the simulation of the dipolar-chemical shift spectra can be found elsewhere (*41−43*).

RESULTS

The structure of LL-37 and its mechanism of membrane disruption were studied using solid-state NMR and differential scanning calorimetry. The majority of the experiments were carried out using LL-37-*U*, synthetic LL-37 with a sequence identical to the biologically active form and no isotopic labels. CD spectroscopy was used to confirm that this synthetic peptide behaved as reported previously in the literature (*18, 19, 25, 26*), exhibiting a random coil structure in pure water and a primarily helical signature in the presence of anions or lipids at micromolar peptide concentrations (data not shown). A second sample of LL-37, LL-37-*L*, was synthesized incorporating site-specific isotopic labels: ^{15}N-Val$_{21}$, ^{13}C=O-Leu$_{31}$, and ^{13}C$_\alpha$-Ala$_{13}$. This labeling scheme places an ^{15}N label in the middle of the proposed amphipathic, α-helical region of the peptide, which extends from residues 11−32 based on estimates of the helical content from CD spectra and sequence analysis of the peptide. The ^{15}N label is useful for determining the orientation of the α-helix in lipid bilayers. The two ^{13}C labels are placed near either end of the helical region and used to confirm the extent of the helix. To enable easy resolution and assignment in the doubly ^{13}C-labeled peptide, one ^{13}C$_\alpha$ and one ^{13}C=O label were used. Alanine was substituted for isoleucine at residue 13 due to the limited availability of ^{13}C$_\alpha$-labeled Fmoc amino acids.

Secondary Structure of LL-37. To check that the single amino acid substitution did not alter the secondary structure of the peptide, CD spectra of the labeled and unlabeled LL-37 samples were compared in the presence of lipids (both DMPC and 4:1 DMPC/DMPG) at different peptide/lipid mole ratios in both water and phosphate buffer. A sample pair of CD spectra for both LL-37-*L* and LL-37-*U* in DMPC SUVs in phosphate buffer is shown in Figure 1. The spectra are the same with clear minima at 208 and 222 nm, indicating that both LL-37-*L* and LL-37-*U* are primarily α-helical in lipid vesicles, and have the same degree of helicity. The same
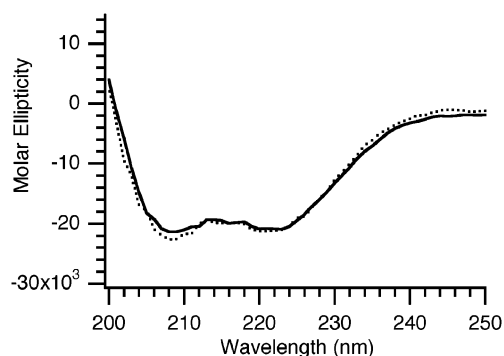
FIGURE 1: CD spectra of LL-37-*U* (solid line) and LL-37-*L* (dotted line) in lipid SUVs in phosphate buffer at a LL-37/DMPC mole ratio of 1:25 ratio and 2 μM LL-37 concentration. There is no difference between the CD spectra of LL-37-*U* and LL-37-*L* in the presence of DMPC.
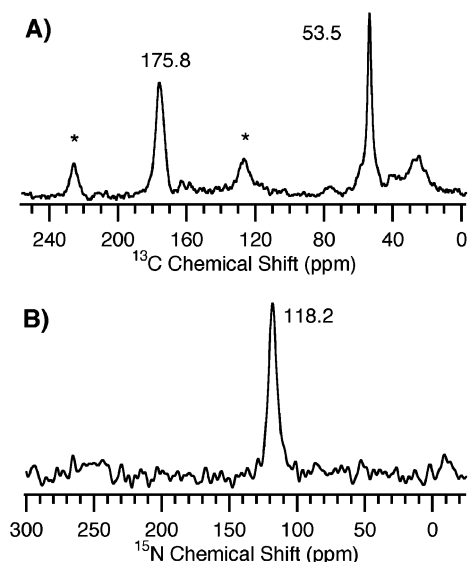

FIGURE 2: (A) ^{13}C CPMAS spectrum of LL-37-*L* dry powder with 5 kHz MAS at 35 °C. The peaks at 175.8 and 53.5 ppm correspond to the ^{13}C=O Leu$_{31}$ and ^{13}C$_\alpha$ Ala$_{13}$ site-specific isotopic labels, respectively. The chemical shift ranges characteristic of α-helix and β-sheet for leucine carbonyl are 173.8−177.6 ppm and 170.5−174.4 ppm, respectively. For alanine C$_\alpha$ the typical ranges are 52−54.1 ppm for α-helix and 47.5−52 ppm for β-sheet. The peaks marked with an asterisk are spinning sidebands. The remaining peaks are natural abundance background signal from the rest of the peptide. (B) ^{15}N CPMAS spectrum of LL-37-*L* dry powder with 5 kHz MAS at 35 °C; the peak is at 118.2 ppm. Chemical shifts between 122 and 129 ppm are characteristic of valine ^{15}N in β-sheet, while chemical shifts lower than 122 ppm are characteristic of an α-helix.

results were obtained for all such pairs of samples comparing LL-37-*L* and LL-37-*U* in either type of lipid and at various peptide:lipid mole ratios (data not shown), confirming that there is no difference in behavior between the two peptides.

Figure 2A shows the ^{13}C CPMAS spectrum of LL-37-*L* as a dry powder. The sample was prepared by lyophilizing the peptide from water at a concentration of about 200 μM, conditions under which the peptide is helical and aggregated in solution. The single intense peaks in the ^{13}C=O and ^{13}C$_\alpha$ regions are from the site-specific labels at Leu$_{31}$ and Ala$_{13}$, respectively. Backbone ^{13}C isotropic chemical shifts are sensitive to the secondary structure of the peptide at each residue (*44−48*). The Leu$_{31}$ ^{13}C=O peak at 175.8 ppm and the Ala$_{13}$ ^{13}C$_\alpha$ peak at 53.5 ppm are both within the ranges

typical of α-helical structure. The ^{15}N isotropic chemical shift is also sensitive to peptide secondary structure (*45, 49*) and is 118.2 ppm for ^{15}N-labeled Val$_{21}$ in LL-37-*L* (Figure 2B). This is consistent with the amphipathic α-helix extending from residues 13 to 32 as predicted.

Orientation of LL-37 in Lipid Bilayers. The orientation of LL-37 in a variety of lipid bilayers was determined from ^{15}N chemical shift spectra of LL-37-*L* in oriented bilayer samples. Interpretation of ^{15}N chemical shift spectra of aligned samples requires knowledge of both the magnitude and orientation of the chemical shielding tensor in the molecular frame. These parameters were determined from spectra of a dry powder sample of LL-37-*L* (Figure 3A,D) since the chemical shielding tensor is primarily sensitive to the local peptide sequence and secondary structure and the α-helix in which Val$_{21}$ is located is very stable and is maintained under a wide range of conditions. Use of a solid sample eliminates motion of the peptide that occurs in a fluid bilayer and can interfere with acquisition of spectra; it also improves S/N since larger quantities of peptide can be used when lipids and water are not included in the sample volume. The principal values of the ^{15}N-Val$_{21}$ chemical shielding tensor were determined to be 54.5 ± 2 ppm, 78.5 ± 2 ppm, and 221 ± 2 ppm from the best fitting simulation of the powder pattern (Figure 3A). A 1-D dipolar-shift powder pattern, shown in Figure 3D, was used to determine the orientation of the chemical shielding tensor relative to the ^{15}N−^{1}H bond. The values of α and β, the angles which define the orientation of the ^{15}N−^{1}H dipolar vector in the principal axis system of the chemical shielding tensor (see Figure 3F), were determined by simulating the dipolar-shift powder spectrum as described in Experimental Procedures. The best fit was obtained with β equal to 19 ± 2°, α equal to 20 ± 15°, and a dipolar coupling of 10.1 ± 0.5 kHz. This dipolar coupling corresponds to an ^{15}N−^{1}H bond length of 1.07 ± 0.02 Å. These values for the ^{15}N−^{1}H bond length and orientation of the ^{15}N chemical shift tensor are very similar to those observed for specifically ^{15}N-labeled residues in magainin and pardaxin (*42, 43, 50*). The line shape depends strongly on the strength of the dipolar coupling and the angle β so these parameters are determined precisely with this method, but α cannot be determined as precisely because the line shape varies only slightly with α for small values of β, as is the case here (*42, 43*). These parameters, determined from the solid powder spectra, were used to interpret the spectra of LL-37-*L* in oriented lipid bilayers. LL-37 is helical in a lipid environment, and is likely to be helical in the solid state as well under the conditions with which the sample was prepared. Even if the secondary structure is lost in the solid, the chemical environment of the ^{15}N nucleus is the same in both samples, as confirmed by the similarity between the powder patterns obtained in the solid (Figure 3A) and lipid environments (Figure 3C). A slight difference in the chemical shift principal values (which cannot be determined accurately from the lipid-associated sample due to the low signal-to-noise ratio) would have a minor effect in the calculation of the exact angle of peptide orientation, but does not affect the interpretation of the results in terms of surface versus transmembrane orientation.

For a residue in an α-helix, such as Val$_{21}$, the orientation of the peptide in lipid bilayers can be determined from the
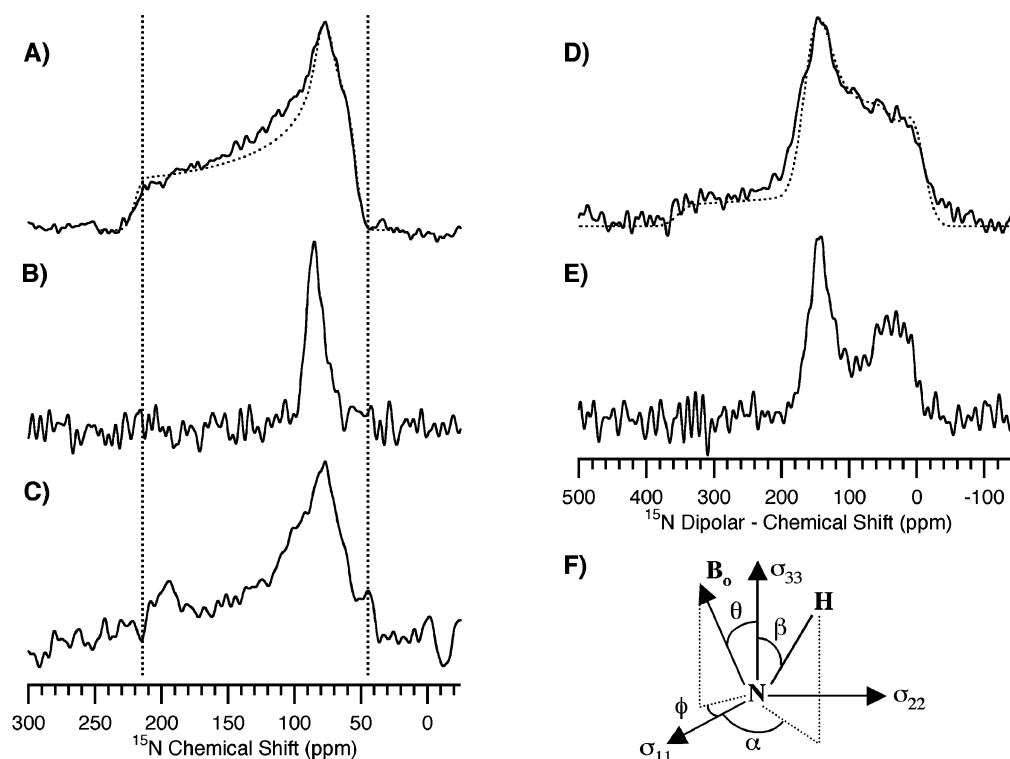
FIGURE 3: ^{15}N chemical shift and dipolar shift spectra of LL-37-*L* (^{15}N label at Val$_{21}$). (A) Chemical shift powder pattern spectrum of dry LL-37-*L*. On the basis of the simulation (dotted line), the principal values of the shielding tensor are 54.5, 78.5, and 221 ppm. Chemical shift spectra of 2 mol % LL-37-*L* in (B) oriented DMPC bilayers with the bilayer normal parallel to the magnetic field and (C) unoriented DMPC bilayers. (D) Dipolar-chemical shift powder pattern of dry LL-37-*L*; simulated spectrum (dotted line) for 10.1 kHz dipolar coupling, $\alpha = 20°$, $\beta = 19°$. (E) Dipolar-chemical shift spectrum of 2 mol % LL-37-*L* in oriented DMPC bilayers with the bilayer normal parallel to the magnetic field. (F) Orientation of the magnetic field and ^{15}N-^{1}H dipole with respect to the principal axis system of the chemical shift tensor.

chemical shift spectrum of an oriented sample. Since the ^{15}N–^{1}H bond is nearly parallel to the helix axis and to σ_{33}, a chemical shift near σ_{33} (>200 ppm) is indicative of the ^{15}N–^{1}H bond and helix axis oriented parallel to the magnetic field, while a chemical shift near σ_{11} and σ_{22} (≤ 100 ppm) is observed when the ^{15}N–^{1}H bond and helix axis are perpendicular to the magnetic field. All of the mechanically oriented samples are aligned with the bilayer normal parallel to the magnetic field, so the former corresponds to a transmembrane peptide orientation and the latter to a surface-oriented peptide. The ^{15}N chemical shift spectrum of a mechanically oriented sample containing LL-37-*L* in DMPC bilayers is shown in Figure 3B. The hydration and alignment of all oriented samples were confirmed with ^{31}P NMR and the ^{31}P spectra are discussed below. There is a single peak near 85 ppm in the ^{15}N spectra of LL-37-*L* in oriented DMPC, indicating that the LL-37 helix is perpendicular to the magnetic field, and is therefore located on the surface of the bilayer in DMPC. The exact location of the peak in the oriented spectrum depends on both the orientation of the peptide and its motion. Figure 4 shows the values of the angles θ and ϕ (defined in Figure 3F) that are consistent with the oriented chemical shift of 85 ppm, assuming that there is minimal motional averaging of the static CSA tensor determined above. The results show that σ_{33} is tipped 65–80° relative to the magnetic field, or 10–25° relative to the surface of the bilayer. Motion of the peptide in the hydrated lipid bilayer that narrowed the powder pattern could also result in the observed peak at 85 ppm with less tilt. The ^{15}N chemical shift powder pattern obtained from 2% LL-37-*L* in hydrated
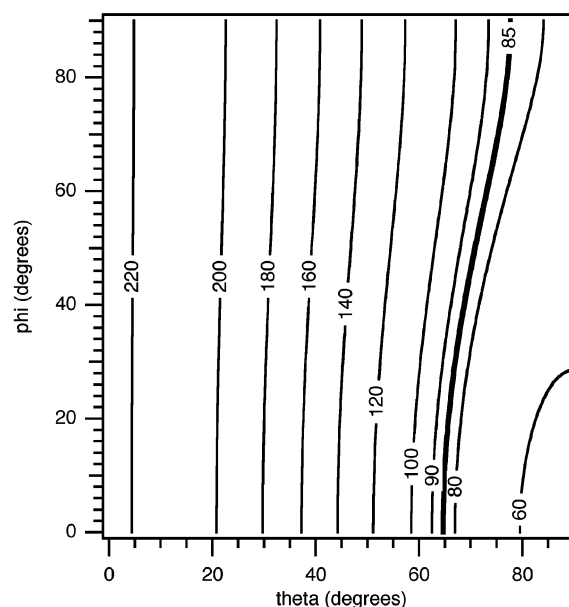

FIGURE 4: Calculated chemical shifts for all possible orientations of LL-37 with respect to the magnetic field using the principal values of the CSA determined from the powder spectrum and eq 2. The observed chemical shift of 85 ppm for LL-37-*L* in bilayers oriented with the bilayer normal parallel to the magnetic field indicates that the peptide helix is oriented roughly parallel to the bilayer surface, but is tilted 10°–25° relative to the surface.

DMPC MLVs is shown in Figure 3C. The signal-to-noise ratio is poor because of limited sample and peptide motion, but the powder pattern is not significantly narrower in the

lipid MLVs than in the dry peptide powder indicating that there is limited motion of the peptide on the millisecond time scale under these conditions. When the sample was aligned with the bilayer normal perpendicular to the magnetic field, no signal was observed (data not shown). This can be explained either by motion of the peptide on the NMR time scale or a distribution of the peptide orientations on the bilayer surface. Since the bilayer surface is a two-dimensional fluid), peptide helices embedded in the bilayer surface may point in any direction, resulting in a very broad powder-pattern-like peak in the perpendicular orientation, which would have very low S/N. The LL-37 helix cannot be undergoing rapid rotation about the bilayer normal, as has been reported for other peptides (*51*), since under those conditions significant averaging of the CSA is observed in a MLV environment and a single peak at the averaged chemical shift is observed. Therefore, the lack of signal from perpendicularly oriented samples is due to the small sample size and low S/N of the broad powder pattern expected for the variety of possible peptide orientations on the bilayer surface.

The 1-D dipolar-shift spectrum of 2% LL-37-*L* in oriented DMPC bilayers (Figure 3E) is also consistent with a surface orientation of the LL-37 helix. The splitting between the two peaks in the 1-D dipolar-shift spectrum is proportional to the dipolar coupling, as described in Experimental Procedures. The dipolar splitting observed for LL-37-*L* oriented in DMPC bilayers with the bilayer normal parallel to the magnetic field is 7.4 kHz. Compared to the full dipolar coupling of 10.1 kHz determined above from the dipolar-chemical shift powder pattern, this indicates that the $^{15}N-$$^{1}H$ bond is tipped $73 \pm 2°$ from the magnetic field direction, or $17 \pm 2°$ from the plane of the bilayer, assuming no peptide motion. These spectra confirm that LL-37 is oriented on the surface of the bilayer as was determined from the chemical shift spectra.

The effects of temperature, peptide concentration, lipid composition, and the presence of ions in the aqueous phase on the orientation of LL-37 in hydrated lipid bilayers were investigated, and ^{15}N chemical shift spectra are shown in Figures 5−7 (all samples aligned with the bilayer normal parallel to the magnetic field). Despite their potential to alter the orientation of LL-37 in the bilayer, none of these factors had any effect on LL-37 orientation as shown below.

No change in the position or width of the peak was observed over the temperature range studied (35−50 °C) in any of the samples, indicating that the surface orientation of LL-37 was maintained under these conditions (Figures 5 and 6). However, the relative intensity of the LL-37 peak does decrease with temperature, resulting in worse S/N at higher temperatures. This is most easily seen in the POPE spectra (Figure 6) where the natural abundance ^{15}N signal from the ethanolamine headgroup (Figure 6A, near 30 ppm) provides a standard for comparison. This decreased signal at higher temperatures is most likely due to increased motion of LL-37 that interferes with cross-polarization when the bilayer is more fluid. The effect of LL-37 concentration is also shown in Figure 6. Increasing the LL-37 concentration from 2 to 5% does not result in any change in the ^{15}N chemical shift spectrum of LL-37-*L* in POPE, verifying that the surface orientation of LL-37 remains at even higher peptide concentrations.
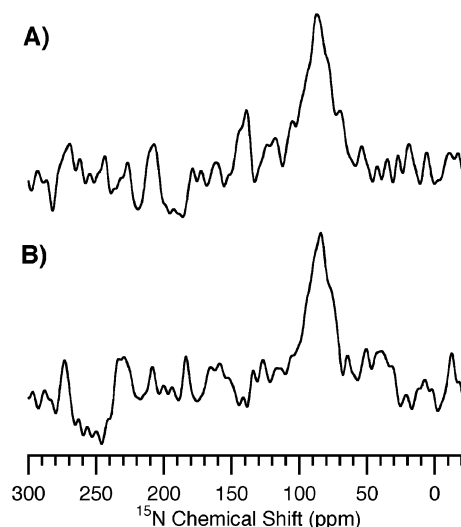

FIGURE 5: ^{15}N chemical shift spectra of 2 mol % LL-37-*L* (^{15}N label at Val$_{21}$) in oriented DMPC bilayers with the bilayer normal parallel to the magnetic field at (A) 35 °C and (B) 50 °C. The surface orientation of LL-37 is the same at both temperatures.
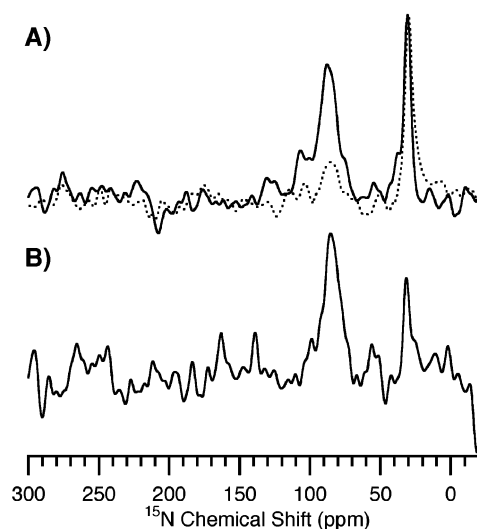

FIGURE 6: ^{15}N chemical shift spectra of POPE oriented bilayer samples showing that increasing LL-37 concentration does not alter its orientation in the bilayer. (A) Spectra of 2 mol % LL-37-*L* in POPE at 35 °C (solid line) and 50 °C (dotted line). (B) Spectrum of 5 mol % LL-37-*L* in POPE at 35 °C. The peak near 30 ppm is due to natural abundance ^{15}N in the ethanolamine headgroups of the lipids.

The role of electrostatic interactions is shown in Figure 7. When DMPC bilayers containing 2% LL-37-*L* were hydrated with tris buffer (10 mM tris, 100 mM NaCl, 2 mM EDTA, pH 7.4) instead of deionized water (Figure 7A), the ^{15}N chemical shift of the labeled peptide in mechanically aligned bilayers was still 85 ppm (compare with the water-hydrated samples in Figure 5). This demonstrates that the surface orientation of LL-37 in the lipid bilayer is identical in the presence or absence of aqueous ions. The ^{15}N chemical shift peak also remained at 85 ppm upon addition of negatively charged lipids to the bilayer as shown in the spectra of 2% LL-37-*L* in 4:1 DMPC/DMPG (Figure 7B) and 4:1 POPC/POPG (Figure 7D) hydrated with water. This indicates that the same surface orientation of LL-37 is maintained in both negatively charged and zwitterionic lipid bilayers.
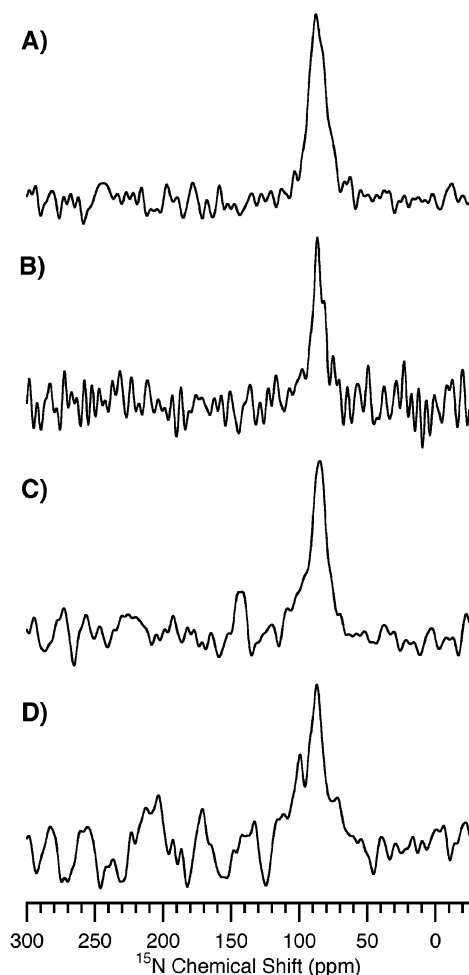
FIGURE 7: The presence of negatively charged lipids or hydration of the bilayer with ion-containing buffer does not alter the ^{15}N chemical shift and orientation of LL-37 in the bilayer. (A) Spectrum of 2 mol % LL-37-*L* in tris-buffer-hydrated DMPC at 50 °C. (B) Spectrum of 2% LL-37-*L* in water-hydrated 4:1 DMPC/DMPG at 50 °C. (C) Spectrum of 2 mol % LL-37-*L* in water-hydrated POPC at 35 °C. (D) Spectrum of 2 mol % LL-37-*L* in water-hydrated 4:1 POPC/POPG at 35 °C.

The PE headgroup is more common in bacterial membranes, while the PC headgroup is prevalent in eukaryotic outer membranes. The ^{15}N chemical shift and surface orientation of 2% LL-37-*L* in POPE (Figure 6A) exactly matches the results obtained in DMPC and POPC bilayers (Figures 5 and 7). Comparison of the results for LL-37 in DMPC with those in POPC and POPE also demonstrates that the surface orientation is the same whether the acyl chains are saturated or contain a single unsaturation. These results show that LL-37 orients along the surface of the bilayer under all the conditions studied, regardless of peptide concentration, lipid composition, temperature, or the presence of aqueous ions, ruling out the formation of barrel-stave pores.

Perturbation of the Lipid Bilayer by LL-37—^{31}P NMR. The effect of LL-37 on the lipid headgroup was investigated using ^{31}P solid-state NMR of oriented samples with the bilayer normal aligned parallel to the magnetic field for all samples unless otherwise noted. The ^{31}P spectrum of pure DMPC bilayers hydrated with water at 35 °C (solid line) and 50 °C (dotted line) are shown at the top of Figure 8A. Both spectra have a single narrow peak at the parallel edge of the L$_\alpha$-
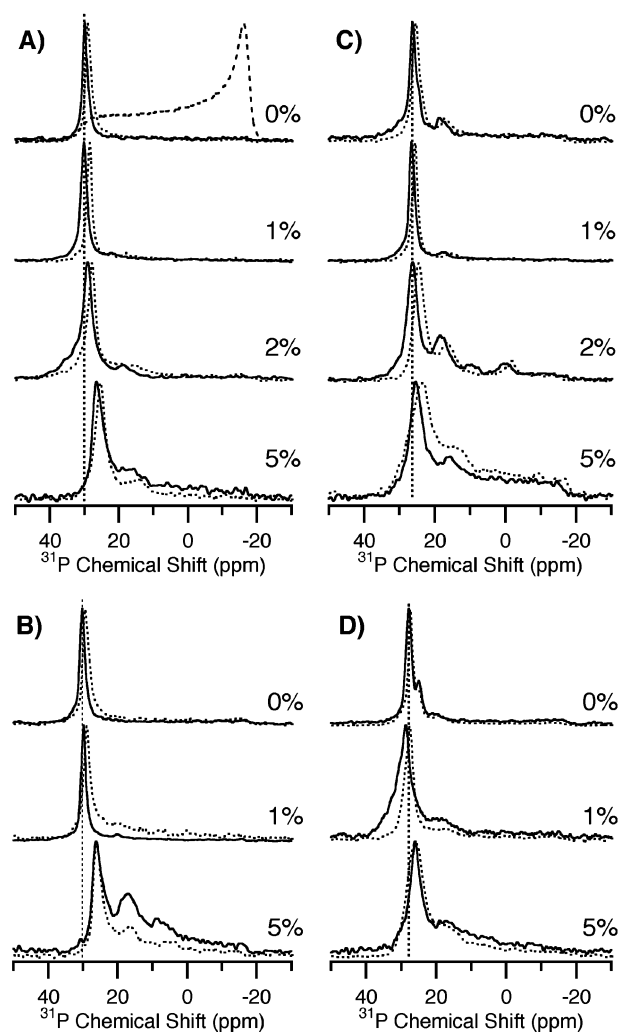

FIGURE 8: ^{31}P spectra of oriented bilayer samples (bilayer normal parallel to the magnetic field) showing the effect of negatively charged lipids and hydration with ion-containing buffer on the ability of LL-37 to perturb the lipid headgroup. Spectra of (A) DMPC hydrated with water, (B) DMPC hydrated with tris buffer (10 mM tris, 100 mM NaCl, 2 mM EDTA, pH 7.4), (C) 4:1 DMPC/DMPG hydrated with water, and (D) 4:1 DMPC/DMPG hydrated with tris buffer were obtained at 35 °C (solid lines) and 50 °C (dotted lines) with the indicated LL-37 concentrations (mole%). The experimental ^{31}P powder pattern of unoriented DMPC MLVs is shown as a dashed line in (A) for comparison.

phase DMPC powder pattern (Figure 8A, dashed line), indicating that all the lipids are well aligned with no residual powder pattern characteristic of unoriented lipids. At the higher temperature, there is a slight shift ($\approx$1 ppm) toward lower frequency of the aligned peak as expected due to increased motional narrowing of the CSA, but the spectra are otherwise identical. No change is observed when the bilayer includes 1% LL-37 and the lipids remain well oriented at both temperatures. With 2% LL-37 incorporated in the bilayer, the oriented peak is slightly broader, indicating that the presence of 2% LL-37 causes some of the lipid headgroups to change conformation or become tilted relative to the unperturbed bilayer. In the 5% LL-37 samples, the oriented peak is further broadened and shifted to lower frequency at both 35 and 50 °C, which may reflect increased tilt or wobbling motion of the headgroup. There is also a small peak near 15 ppm and a low intensity broad component that extends across the base of the spectra representing

unaligned lipids; however, the shape of this unaligned component is not that of a typical powder pattern and it is discussed further below.

Oriented DMPC bilayers were also directly hydrated with tris buffer (Figure 8B) to test whether the presence of ions, known to affect the structure and aggregation state of LL-37 in solution (*18*), also affect its interaction with lipids. For DMPC with 0% or 1% LL-37, the ^{31}P spectra obtained with either hydration method are identical (Figure 8A,B) indicating that these samples are insensitive to low salt concentrations. At 5% LL-37, the samples hydrated with tris buffer (Figure 8B) are similar to those hydrated with water except that there are additional peaks at about 9 and 18 ppm. These peaks may each represent distinct populations of lipids with different headgroup tilt, or the peaks at 27 and 9 ppm may represent different domains with the peak at 18 ppm arising from exchange between them. However, no cross-peaks were observed when 2-D ^{31}P exchange experiments were performed with mixing times up to 600 ms (data not shown), so the former explanation is more likely. The unoriented components of the spectra in samples hydrated with either water or tris buffer are also less at 50 °C than at 35 °C (Figure 8A,B).

The effect of LL-37 on the ^{31}P spectra of oriented 4:1 DMPC/DMPG bilayers at 35 and 50 °C with water or tris buffer hydration is shown in Figure 8C,D. In the case of the pure lipid bilayers, two peaks are resolved at both temperatures in the presence of salt (Figure 8D, top), while samples hydrated with water alone (Figure 8C, top) have a slight shoulder. There is also a 2 ppm difference between the oriented peak in water-hydrated and tris-buffer-hydrated samples, showing that the addition of charged lipids makes the bilayer more sensitive to the presence of salt. The area of the two resolved peaks in the pure lipid spectra in Figure 8C,D is not exactly equal to the 4:1 ratio of DMPC to DMPG present in the sample, but the smaller peak is assigned to DMPG-rich regions and the larger peak to DMPG-poor regions on the basis of the relative amount of each lipid in the sample. LL-37 prevents this domain separation since these domains are not discernible when LL-37 is present in the sample, regardless of hydration method as seen in Figure 8. At 1% LL-37 in the samples hydrated with tris buffer (Figure 8D) the single oriented peak has the chemical shift of the DMPG-poor peak in the pure lipid samples. 1% LL-37 causes a broadening of the oriented peak in the tris buffer-hydrated samples, demonstrating that there is tilt or a change in conformation of the headgroup as was seen in water-hydrated DMPC at higher (2%) LL-37 concentrations (Figure 8A). At 2% LL-37 in 4:1 DMPC/DMPG bilayers hydrated with water (Figure 8C), there are additional peaks at about 0 and 18 ppm at both temperatures and also a small peak near 10 ppm at 35 °C. These peaks are much larger than in the DMPC samples containing 2% LL-37 and are most similar to those seen in DMPC with 5% LL-37 and tris buffer hydration (Figure 8B). As expected, these results show that cationic LL-37 interacts more strongly with negatively charged bilayers than zwitterionic bilayers, requiring less peptide for the same amount of perturbation. At 5% LL-37, there is a large increase in the broad, unaligned component in the water-hydrated 4:1 DMPC/DMPG samples (Figure 8C), but the peaks present in the 2% LL-37 sample are much

less distinct. There is a similar but much smaller increase of the broad, unaligned component in the tris-buffer-hydrated samples.

Overall, the ^{31}P spectra report moderate changes in the headgroup of oriented DMPC and 4:1 DMPC/DMPG bilayers in the presence of LL-37. The slight shift of the oriented peak toward lower chemical shift with increasing LL-37 concentration reflects a slight change in headgroup tilt or wobble, since the residual unoriented component in the 5% LL-37 samples indicates that the CSA is not narrowed by motional averaging. Assuming that the headgroups have a single tilt angle, this shift is accounted for by a tilt of about 16° away from the bilayer normal in the DMPC samples and less than 8° in 4:1 DMPC/DMPG samples. The headgroup tilt required to produce the peak at 15−18 ppm found in the higher LL-37 concentration samples is about 30°. If this peak reflects lipid headgroups that are wobbling, or are moving rapidly over a nonlamellar lipid surface, the range of angles covered must be larger than 30°.

The effect of LL-37 on bilayers with other lipid compositions was also investigated using ^{31}P NMR spectroscopy, and the results are shown in Figure 9. The most striking feature of these spectra is the limited effect of LL-37 on the lipid headgroups, even at concentrations of 5%. In Figure 9A, the effect of increasing LL-37 concentrations on POPC is shown. There is broadening of the oriented peak, but almost no unoriented component, even at the highest peptide concentrations. In 4:1 POPC/POPG bilayers (Figure 9B), the pure lipid spectrum has a shoulder on the main peak, which becomes less resolved as the LL-37 concentration increases, as was seen for DMPC/DMPG bilayers (Figure 8C,D). Since bilayers composed of POPC and POPG have a single unsaturated bond in the SN-2 acyl chain, they are more fluid than DMPC and DMPG bilayers which have only fully saturated acyl chains. The ^{31}P spectra in Figures 8 and 9 show that LL-37 induces headgroup distortion or nonlamellar lipid structures in a larger percentage of the lipids in the more rigid, fully saturated bilayers. Disruption of the bilayer also decreases slightly when the temperature, and consequently the fluidity, of fully saturated DMPC bilayers increases (Figure 8). This pattern is supported by the spectra in Figure 9C as well, which show the ^{31}P spectra of 4:1 POPC/cholesterol bilayers with varying amounts of LL-37. There is significant broadening of the oriented peak and formation of an unoriented component, as in DMPC (Figure 8). Cholesterol increases the rigidity of the fluid lamellar bilayer and the effect of the peptide on the lipid headgroup is much greater than in POPC alone.

In POPE (Figure 9D) and 4:1 POPE/POPG (Figure 9E), LL-37 has a greater effect on the lipid headgroup at intermediate concentrations (1−2%) than at high concentrations (5%) as shown by the broadening of the oriented peak and intensity of the unoriented component. This suggests that extensive peptide aggregates form at these high concentrations so that fewer lipids are actually perturbed. High LL-37 concentrations also lead to resolution of two oriented components in POPE/POPG bilayers (Figure 9E), the opposite of the effect observed in DMPC/DMPG (Figure 8C,D) and POPC/POPG (Figure 9B). In zwitterionic bilayers, disruption of POPE (Figure 9D) is greater than disruption of POPC, particularly at 1−2%. These differences demonstrate that the interaction of LL-37 with both anionic and
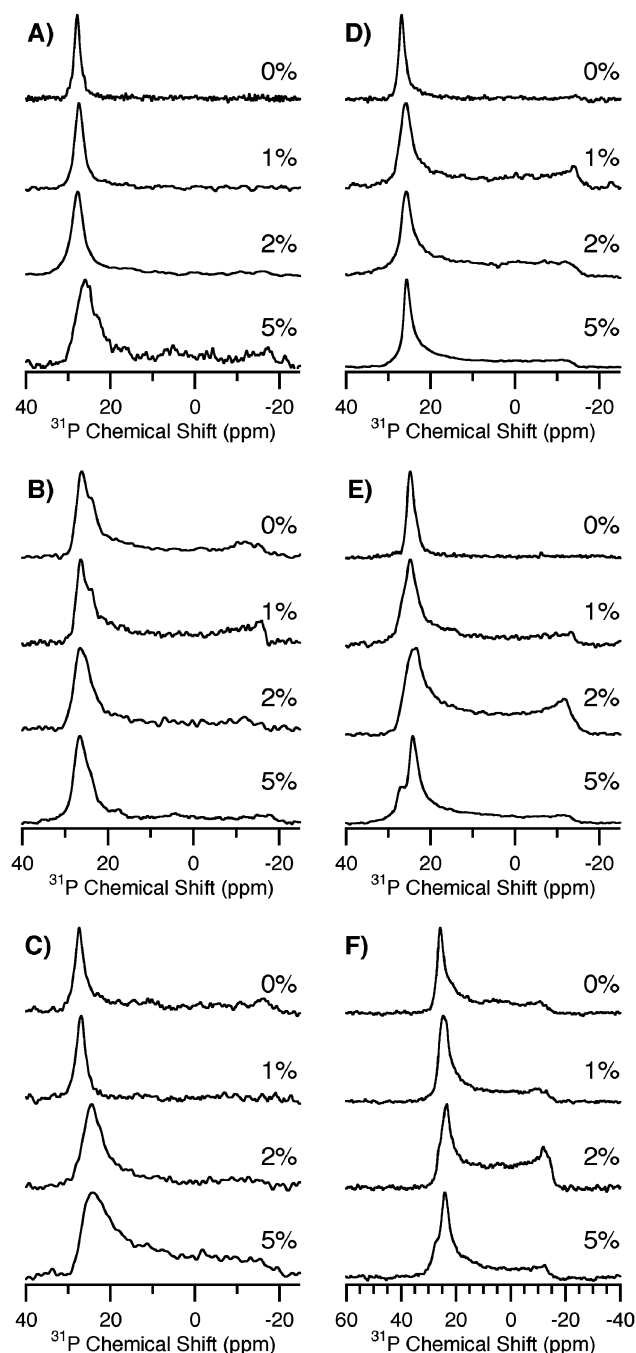
FIGURE 9: ³¹P spectra of oriented bilayer samples showing the effect of increasing LL-37 concentration (mole%) on the lipid headgroup in bilayers with a variety of lipid compositions. The spectra are of (A) POPC, (B) 4:1 POPC/POPG, (C) 4:1 POPC/cholesterol, (D) POPE, (E) 4:1 POPE/POPG, (F) *E. coli* lipids at 35 °C.

FIGURE 10: LL-37 inhibits the formation of negatively curved inverted hexagonal phase in POPE. (A) ³¹P chemical shift spectra of oriented POPE bilayers with 5 mol % LL-37 at increasing temperatures. The dotted spectrum is of pure POPE in the absence of any LL-37 at 70 °C. Both samples were aligned with the glass plate normal parallel to the magnetic field. (B) ³¹P spectrum of POPE containing 2 mol % LL-37 at 80 °C with the glass plate normal parallel to the magnetic field (top) and perpendicular to the magnetic field (bottom) with the simulated spectra of oriented hexagonal phase shown for each orientation as a dotted line.

cardiolipin, and 17.6% other lipid types by weight. In particular, the greatest disruption is again observed at intermediate LL-37 concentrations where there is a large unoriented component present, and by 5% LL-37 this unoriented component has decreased greatly, but two oriented components become resolved. These results show that in a variety of model lipid bilayers and actual *E. coli* lipids LL-37 is capable of perturbing the structure of oriented bilayers but does not induce the formation of an isotropic peak characteristic of micelles, ruling out a detergent-like mechanism of bilayer fragmentation.

Induction of Positive Curvature Strain in Lipid Bilayers by LL-37. The toroidal pore model of lipid bilayer disruption by antimicrobial peptides depends on the induction of curvature strain in the bilayer by the peptides to form the toroidal peptide−lipid pore. A combination of ³¹P NMR and differential scanning calorimetry (DSC) was used to investigate the ability of LL-37 to induce curvature strain in lipid bilayers. Figure 10 illustrates the ability of LL-37 to inhibit the fluid lamellar (L_α) to inverted hexagonal (H_{II}) phase transition of POPE. When the inverted hexagonal phase is formed from oriented lipid bilayers, the characteristic tubes of this phase are aligned with their main axis parallel to the bilayer surface from which they formed. Since the tubes are narrow enough for rapid lipid diffusion to occur around the tube, a single peak at the average chemical shift of the parallel and perpendicular edges of the lamellar spectrum is observed for a sample aligned with the original bilayer normal parallel to the magnetic field (Figure 10B, top). If the sample is turned so that the original bilayer normal is perpendicular to the magnetic field, then a spectrum is obtained that extends from the chemical shift of the parallel oriented hexagonal phase to the perpendicular edge of the lamellar spectrum (Figure 10B, bottom). This is because hexagonal phase tubes can form in any direction parallel to the bilayer surface. This lack of directional preference leads to a circular distribution, the 2-dimensional equivalent of the spherical powder distribution. The dotted lines in Figure 10B

zwitterionic lipids is influenced by the headgroup size of the major component of the bilayer.

Model lipid bilayers enable the testing of the importance of various features such as lipid charge, acyl chain saturation, or headgroup type on the interaction of LL-37 with the lipid headgroup, but it is also necessary to examine the behavior of LL-37 in a more biologically relevant environment in order to understand its function. The effect of LL-37 on *E. coli* lipids is shown in Figure 9F. The spectra are very similar to those obtained in POPE/POPG bilayers (Figure 9E), which is not surprising since the lipid composition of the *E. coli* lipid extract is 57.5% PE lipids, 15.1% PG lipids, 9.8%
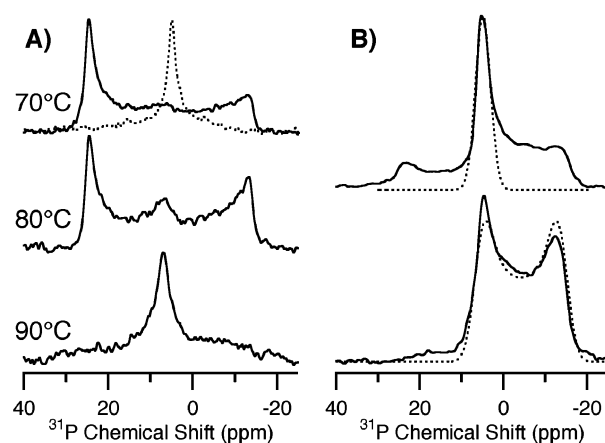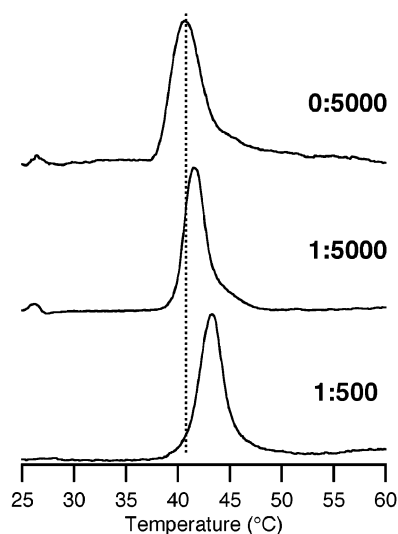
FIGURE 11: Differential scanning calorimetry of the lamellar to inverted hexagonal phase transition of DiPoPE shows that LL-37 inhibits the formation of inverted hexagonal phase and raises the phase transition temperature at the low peptide-to-lipid ratios of 1:5000 and 1:500.
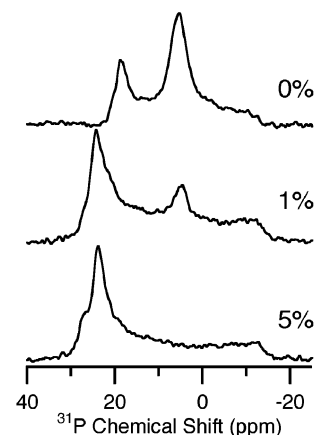

FIGURE 12: LL-37 inhibits the formation of negatively curved inverted hexagonal phase in the physiological mixture of lipids found in *E. coli* membranes. ^{31}P chemical shift spectra of oriented *E. coli* bilayers at 50 °C show significant inverted hexagonal phase formation (peak near 5 ppm), but increasing concentrations of LL-37 reduce and eliminate this peak from the spectrum.
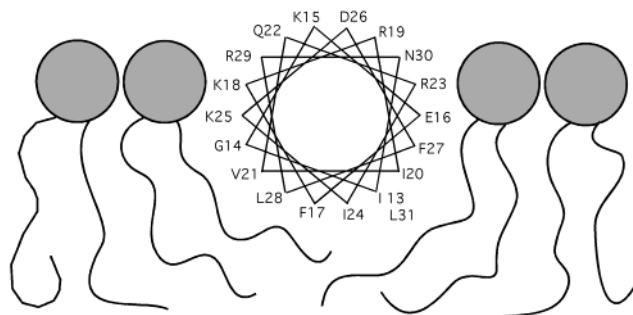

FIGURE 13: Cartoon showing the location of LL-37 in the membrane interface.

are spectra simulated for pure oriented inverted hexagonal phase formed from aligned bilayers in either orientation.

The dotted line in Figure 10A is the spectrum of pure POPE which undergoes the L_α to H_{II} phase transition near 70 °C and has a single peak at about 5 ppm characteristic of an oriented inverted hexagonal phase. The phase transition is observed at 72 °C using DSC, but temperature cannot be determined as precisely within the spectrometer during acquisition. The spectra shown in Figure 10A with solid lines correspond to POPE with 5% LL-37 incorporated. At 70 °C, all of the lipids remain in the lamellar phase, and the transition to the inverted hexagonal phase is not complete until 90 °C, 20 °C above the phase transition temperature of the pure lipid. This demonstrates that LL-37 inhibits the L_α to H_{II} phase transition suggesting LL-37 induces positive curvature strain in the membrane. Panel B of Figure 10 confirms that the lipid peak at 5 ppm observed in the presence of LL-37 is due to formation of a hexagonal phase and not merely tilting of the lipid headgroups. The solid line spectra in Figure 10B are of POPE with 2% LL-37 at 80 °C. The parallel (Figure 10B, top) and perpendicular (Figure 10B, bottom) orientations of the sample produce spectra that match the simulated spectra for pure oriented hexagonal phase in each orientation, although there is an additional unoriented lipid component in the parallel orientation. These spectra show that moderate to high concentrations of LL-37 induce significant positive curvature strain in the lipid bilayer, and that the effect increases with increasing peptide concentration.

The same results are obtained for much lower concentrations of LL-37 using DSC. DiPoPE undergoes the L_α to H_{II} phase transition near 41 °C. Figure 11 shows that as little as 3 μM LL-37 in a 1:5000 peptide/lipid mole ratio induces an observable increase in the transition temperature. Even at these low concentrations, which are directly comparable to the MIC of LL-37 against *E. coli*, LL-37 inhibits the L_α to H_{II} phase transition and induces positive curvature strain. The physiological relevance of the ability of LL-37 to induce curvature strain in the lipid bilayer was further confirmed

by examining the effect of LL-37 on *E. coli* lipids directly. ^{31}P spectra of oriented *E. coli* lipids at 50 °C are shown in Figure 12. When no LL-37 is present, a significant non-lamellar peak is observed at the chemical shift characteristic of oriented hexagonal phase ($\approx$5 ppm, see Figure 10). Increasing concentrations of LL-37 suppress this peak to the extent that there is no hexagonal phase peak present at 5% LL-37; only oriented and unoriented lamellar components are visible in the spectrum. Since the *E. coli* lipids have a high percentage of PE, the peak at 5 ppm is most likely due to formation of inverted hexagonal phase, with the transition temperature lower than pure POPE due to the additional lipid components in the *E. coli* lipid mixture. This confirms that LL-37 induces positive curvature strain in biologically relevant lipid mixtures, as well as simple model systems.

DISCUSSION

The above data demonstrate that LL-37 forms a stable α-helix that lies at the polar/nonpolar interface on the surface of the bilayer (Figure 13). This surface orientation, which does not change with temperature, lipid headgroup charge, LL-37 concentration, or the presence of aqueous ions, excludes a barrel-stave mechanism of membrane disruption. Although previous work (25) had suggested detergent-like fragmentation of the membrane, the lack of an isotropic peak (or other peak characteristic of a high degree of motional averaging of the ^{31}P CSA) in the ^{31}P spectra eliminates this possibility. Thus, LL-37 must function by initially carpeting

the surface of the membrane and inducing leakage either through the formation of toroidal pores, as supported by the induction of positive curvature strain, or less well-defined membrane defects.

Previous studies in the literature have shown that LL-37 forms a more stable helix than the usual amphipathic, α-helical, antimicrobial peptide, and does not require a membrane surface in order to fold (*18*, *28*). CD experiments have shown that LL-37 is predominantly α-helical in solution as long as anions are present (10−160 mM concentration, depending on the anion), or the concentration of peptide is above 1 μM (*18*). The concentration dependence and cross-linking experiments demonstrate that aggregation of LL-37 stabilizes the helical conformation (*25*). Published CD and IR results (*18*, *25*) and the CD experiments shown here (Figure 1) demonstrate that the helical conformation is maintained in the presence of lipids. Since the helical conformation remains unchanged over a wide range of conditions and is stabilized by aggregation, the same helical structure is expected to remain in the solid state, and this is consistent with the ^{13}C CPMAS experiments (Figure 2). The extent of the helical region has been predicted to range from residues 11−32 based on the percent of helical residues indicated by CD spectra and analysis of the peptide sequence, and the ^{13}C isotropic chemical shifts of ^{13}C=O-Leu$_{31}$ and ^{13}C$_\alpha$-Ala$_{13}$ support this prediction.

LL-37 Does Not Form Barrel-Stave Pores. The orientation of the peptide in the membrane is a key feature distinguishing the barrel-stave model from the rest, and the ^{15}N NMR experiments address this question. The oriented ^{15}N spectra show that the peptide helix is aligned on the surface of the bilayer in a variety of lipid environments, as was predicted for such an amphipathic α-helix (Figures 5−7). The ^{15}N spectra of LL-37 in MLVs indicate that LL-37 does not rotate rapidly about the membrane normal as has been shown to occur for another surface-oriented antimicrobial peptide, ovispirin (*51*). LL-37 is larger than ovispirin, which may slow its rotation. LL-37 also aggregates in solution, and fluorescence studies suggest that LL-37 is partly self-associated when bound to PC membranes (*25*), another factor that would slow rotation of the peptide.

It has been proposed that antimicrobial peptides which lie on the surface may still function by a barrel-stave mechanism through equilibrium with an inserted pore-forming orientation, and that the inserted form is favored by higher peptide concentrations and hydrophobic matching between the bilayer thickness and hydrophobic length of the inserted helix (*7*). Since fluorescence studies showed partial LL-37 aggregation in PC bilayers at a P:L ratio as low as 1:150 (*25*), the 2% LL-37 concentration used for ^{15}N NMR experiments should be high enough for aggregation to occur, and at least some transmembrane oriented peptide should be observed if it functions by the barrel-stave mechanism. Instead, only surface oriented peptide is observed for LL-37 (Figures 5−7), in agreement with a previously published FTIR study on LL-37 at P:L mole ratios of 1:40, 1:80, and 1:120 in PC bilayers (*25*). The oriented chemical shift is also the same at both 35 and 50 °C and at 2 and 5% LL-37 (see Figures 5 and 6). Changing the temperature and the peptide concentration should result in a change in the ^{15}N chemical shift of LL-37-*L* if there was an underlying equilibrium between a surface and inserted form, but no change was observed. The

presence of ions in aqueous solution increases the helicity and aggregation of the highly cationic LL-37 (*18*), but adding negatively charged lipids to the hydrated bilayer or ions to the aqueous phase has no effect on the orientation of LL-37 (see Figure 7). Thus, LL-37 remains in a stable surface orientation and does not insert into a transmembrane orientation, even under conditions suitable for aggregation, ruling out a barrel-stave mechanism for pore formation and membrane disruption.

LL-37 Does Not Fragment the Bilayer in a Detergent-Like Manner. Distinguishing between the remaining mechanisms requires knowledge of how LL-37 perturbs the lipids themselves. The toroidal pore model and detergent-like micelle formation both have an initial step in which peptides carpet the surface of the bilayer, but they differ in how the bilayer structure is disrupted. The ^{31}P NMR experiments provide the necessary insight into the effects of LL-37 on the lipid bilayers to enable the detergent-like model to be ruled out. In the ^{31}P spectra of oriented lipid bilayers with LL-37 incorporated, no isotropic peak characteristic small bilayer fragments such as micelles or small disks was observed (Figures 8 and 9). Isotropic peaks are clearly present in ^{31}P spectra of both oriented and unoriented bilayers perturbed by other peptides which are known to induce micellization of the membrane, such as melittin (*36*), mastoparan (*35*), nisin (*52*), or δ-lysin (*39*). In the case of protegrin-1 (*53*), an isotropic peak was not observed, but significant averaging of the ^{31}P CSA did occur, and was attributed to the formation of small disklike fragments from the membrane. This was also not observed in any of the lipid systems containing LL-37. To confirm that the absence of bulk water in the oriented samples was not preventing membrane fragmentation, a ^{31}P spectrum of 2% LL-37 in DMPC MLVs at a 0.74 μM lipid concentration was obtained (data not shown). A powder pattern was clearly present while no isotropic peak was visible. Thus, the ^{31}P results indicate that LL-37 disrupts the lipid bilayer, but does not break the membrane up into small fragments via a simple detergent-like mechanism under any of the conditions of lipid composition, temperature, or peptide concentration studied in this work.

LL-37 Induces Positive Curvature Strain in Lipid Bilayers. The ^{31}P spectra and DSC scans in PE lipids (Figures 10−12) show that LL-37 does induce positive curvature strain. The small size of the PE headgroup relative to the acyl chains results in a tendency of these lipids to form negatively curved phases. When LL-37 is added, the formation of the negatively curved inverted hexagonal phase by the PE lipids is inhibited. This demonstrates that LL-37 induces positive curvature strain in the bilayer that partially compensates for the intrinsic negative curvature favored by the lipids, resulting in an extended range of stability of the lamellar phase. This ability of LL-37 to induce positive curvature strain was confirmed at concentrations and in lipid environments that are relevant (Figures 11 and 12) for its antibacterial activity. This supports the toroidal pore model of bilayer disruption by LL-37 both in model lipid bilayers and under the conditions in which it naturally functions.

Lipid Properties Affect the Degree of Bilayer Disruption by LL-37. At 2% LL-37, the ^{31}P NMR spectra show that the effect of LL-37 on the lipid headgroups differs between anionic and zwitterionic bilayers (Figure 8), but the surface

orientation of the peptide remains constant (Figures 5 and 7). This implies that the degree of bilayer disruption must be controlled by the depth of helix insertion or variation in local peptide concentration and aggregation state. The importance of aggregation in bilayer disruption by surface oriented peptides has already been recognized, and the general model of activity for these peptides postulates that toroidal pores, or other membrane defects, arise in areas of high local peptide concentration that form transiently through diffusion of the peptide on the bilayer surface (*9*, *54*).

The high net charge of LL-37, +6, and the resulting electrostatic repulsion between peptides limits LL-37 aggregation as shown by the pH and anion dependence of helix formation and aggregation of LL-37 in solution (*18*). Anions screen this peptide−peptide repulsion and enable LL-37 to fold into a helix and aggregate. LL-37 helicity and aggregation state in solution are positively correlated with activity (*18*), indicating that peptide−peptide association and high local peptide concentration are important. In lipid bilayers, similar reasoning holds that electrostatic attraction between LL-37 and negatively charged lipids should lead to regions rich in PG and peptide, and that greater disruption of the lipids should occur in anionic bilayers due to this indirect lipid-mediated peptide aggregation. This is in agreement with the ^{31}P results (Figures 8 and 9) and the moderate selectivity of LL-37 for anionic bacterial membranes over the corresponding zwitterionic bilayers.

These results contrast with fluorescence studies (*25*) which indicate that LL-37 is partly self-associated in zwitterionic PC bilayers but not in negatively charged PC/PS bilayers at P:L mole ratios of 1:150. However, the fluorescent tags attached to the N-terminus of LL-37 may affect its ability to aggregate, since truncation studies suggest that aggregation occurs through the N-terminus (*25*). Also, fluorescence energy transfer may be difficult to observe for transient, indirect aggregation of peptides with lipids in regions of high local peptide and anionic lipid concentration. The experiments presented here also use PG for the anionic lipid headgroup, while the fluorescence experiments used PS and the characteristics of lipids with PG and PS headgroups are significantly different. Although both have a net −1 charge, the relative size of the headgroup, distribution of charge and susceptibility of the lipid to curvature strain differ, resulting in significant variation of peptide−lipid interaction with either type of lipid, as was shown for magainin (*15*).

In addition to aggregation, the depth of insertion of the peptide helix may vary with bilayer properties. Dathe et. al. have used model peptides based on magainin to show that amphipathic α-helical cationic antimicrobial peptide activity and selectivity are based on a complex combination of electrostatic and hydrophobic interactions (*3*, *4*). Their work illustrates the importance of electrostatic interactions in initial peptide−lipid association and selectivity, but also demonstrates that membrane binding and insertion is determined by a balance of electrostatic attraction to the lipid headgroups and hydrophobic interaction with the bilayer core. When the attraction between positively charged residues on the hydrophilic face of the peptide helix and the lipid headgroups is enhanced by the addition of anionic lipids to the bilayer, the peptide is held more tightly to the headgroup region of the lipid bilayer and its penetration into the hydrophobic core is reduced. Both the ^{31}P and ^{15}N results are consistent with this model in which the helix is held higher in the hydrophilic region of the polar/nonpolar interface in anionic lipid bilayers, resulting in increased headgroup perturbation without altering peptide orientation. In bilayers hydrated with buffer, anions in the buffer shield electrostatic interactions, facilitating greater self-association of the cationic LL-37 and increased perturbation in zwitterionic bilayers (Figure 8A,C). In anionic membranes, this electrostatic shielding disrupts the DMPG−LL-37 interactions as well as peptide−peptide repulsion, reducing the membrane perturbation relative to water-hydrated 4:1 DMPC/DMPG (Figure 8B,D).

A number of features observed in the oriented ^{31}P spectra in the presence of LL-37 differ from well-aligned pure lipid bilayers. The peaks between 5 and 20 ppm could be due to changes in lipid headgroup structure or tilting of the lipid headgroups relative to the bilayer normal, but the shape of the broad component is not consistent with any common lipid phase. The experimental evidence presented here favors formation of a toroidal peptide−lipid pore, and the surface of such a pore has a nonlamellar and nonspherical distribution of lipids. Neglecting the area taken up by peptide and assuming that lipids cover the entire pore surface, such a pore would result in a ^{31}P spectrum similar to a reversed powder pattern (high intensity near the parallel edge and low intensity near the perpendicular edge) if the pore was stable on the NMR time scale and the lipids in the pore did not diffuse quickly due to strong peptide−lipid interactions in the pore complex (*55*). If the lipids diffused rapidly through the pore, a peak with a chemical shift between 7 and 20 ppm would be observed in the ^{31}P spectrum depending on the size of the pore. The ^{31}P results are consistent with this interpretation, since all the distinct peaks fall within the expected ranges, and the unoriented components do not have the normal powder pattern shape with high intensity at the low-frequency edge, but instead have the pattern expected from simulation of a toroidal pore. More conclusive simulation of the ^{31}P line shapes would require additional information on lipid headgroup conformation and lipid motion within the pore.

In addition to the presence of anionic lipids or anions in the aqueous phase, temperature, bilayer rigidity, and headgroup size influence LL-37-induced bilayer disruption as observed by ^{31}P NMR (Figures 8 and 9). These factors alter the membrane properties and may affect the depth of the helix in the membrane interface, "aggregation" of LL-37, or the susceptibility of the membrane to curvature strain, and thus alter ability of LL-37 to perturb the bilayer. Although many factors are clearly important in determining the disruption of real membranes, significant disordering of *E. coli* lipids is observed at physiological temperatures (Figure 9) in accord with the known activity of LL-37 against *E. coli*. Interestingly, some bacteria have developed resistance to LL-37 by adding choline headgroups to lipolpolysaccharide in their outer membrane (*24*). Although the mechanism is not clear, the ^{31}P spectra (Figure 9) show that LL-37 is less disruptive to lipids with choline headgroups, such as POPC, than to common bacterial lipids, such as POPE, consistent with a protective role for choline headgroups against bilayer disruption by LL-37.

CONCLUSION

Three basic mechanisms have been proposed for the membrane disrupting activity of amphipathic α-helical antimicrobial peptides, such as LL-37. The ^{15}N spectra of labeled LL-37 in oriented bilayers show that LL-37 is oriented parallel to the bilayer surface, ruling out formation of barrel-stave pores. A detergent-like mechanism in which the membrane is eventually fragmented into micelles or small disks has been suggested as the most likely for LL-37 (25), but the ^{31}P spectra presented here are not consistent with this model. The third model is formation of toroidal peptide–lipid pores due to curvature strain induced by the presence of peptide. This model is consistent with the ^{31}P and DSC results, which show that LL-37 induces positive curvature strain. It is also possible that locally high concentrations of LL-37 disrupt the packing of lipids in the bilayer to such an extent that transient defects form in the membrane hydrophobic barrier, allowing leakage of ions and molecules down the concentration gradient. Further work is underway to characterize the ability of LL-37 to disrupt the acyl chains in the hydrophobic core of the bilayer. On the basis of the experimental results presented here, the mechanism of LL-37 is most like the toroidal-pore model.

ACKNOWLEDGMENT

REFERENCES

1. Zasloff, M. (2002) *Nature 415*, 389–395.
2. Wieprecht, T., Apostolov, O., Beyermann, M., and Seelig, J. (2000) *Biochemistry 39*, 442–452.
3. Dathe, M., and Wieprecht, T. (1999) *Biochim. Biophys. Acta 1462*, 71–87.
4. Dathe, M., Nikolenko, H., Meyer, J., Beyermann, M., and Bienert, M. (2001) *FEBS Lett. 501*, 146–150.
5. Epand, R. M., and Vogel, H. J. (1999) *Biochim. Biophys. Acta 1462*, 11–28.
6. Bechinger, B. (1997) *J. Membr. Biol. 156*, 197–211.
7. Huang, H. W. (2000) *Biochemistry 39*, 8347–8352.
8. Shai, Y. (1999) *Biochim. Biophys. Acta 1462*, 55–70.
9. Oren, Z., and Shai, Y. (1998) *Biopolymers 47*, 451–463.
10. Fox, R. O., and Richards, F. M. (1982) *Nature 300*, 325–330.
11. He, K., Ludtke, S. J., and Huang, J. W. (1995) *Biochemistry 34*, 15614–15618.
12. He, K., Ludtke, S. J., Worcester, D. L., and Huang, H. W. (1996) *Biophys. J. 70*, 2659–2666.
13. Ludtke, S. J., He, K., Heller, W. T., Harroun, T. A., Yang, L., and Huang, H. W. (1996) *Biochemistry 35*, 13723–8.
14. Matsuzaki, K., Murase, O., Fujii, N., and Miyajima, K. (1996) *Biochemistry 35*, 11361–8.
15. Matsuzaki, K., Sugishita, K., Ishibe, N., Ueha, M., Nakata, S., Miyajima, K., and Epand, R. M. (1998) *Biochemistry 37*, 11856–63.
16. Ladokhin, A. S., and White, S. H. (2001) *Biochim. Biophys. Acta 1514*, 253–260.
17. Gudmundsson, G. H., Agerberth, B., Odeberg, J., Bergman, T., Olsson, B., and Salcedo, R. (1996) *Eur. J. Biochem. 238*, 325–32.
18. Johansson, J., Gudmundsson, G. H., Rottenberg, M. E., Berndt, K. D., and Agerberth, B. (1998) *J. Biol. Chem. 273*, 3718–24.
19. Turner, J., Cho, Y., Dinh, N. N., Waring, A. J., and Lehrer, R. I. (1998) *Antimicrob. Agents Chemother. 42*, 2206–14.
20. Tanaka, D., Miyasaki, K. Y., and Lehrer, R. I. (2000) *Oral Microbiol. Immunol. 15*, 226–231.

21. Larrick, J. W., Hirata, M., Zhong, J., and Wright, S. C. (1995) *Immunotechnology 1*, 65–72.
22. Bals, R., Weiner, D. J., Moscioni, A. D., Meegalla, R. L., and Wilson, J. M. (1999) *Infect. Immun. 67*, 6084–6089.
23. Zasloff, M. (1987) *Proc. Natl. Acad. Sci. U.S.A. 84*, 5449–53.
24. Lysenko, E. S., Gould, J., Bals, R., Wilson, J. M., and Weiser, J. N. (2000) *Infect. Immun. 68*, 1664–1671.
25. Oren, Z., Lerman, J. C., Gudmundsson, G. H., Agerberth, B., and Shai, Y. (1999) *Biochem. J. 341*, 501–13.
26. Nagaoka, I., Hirota, S., Yomogida, S., Ohwada, A., and Hirata, M. (2000) *Inflamm. Res. 49*, 73–79.
27. Agerberth, B., Gunne, H., Odeberg, J., Kogner, P., Boman, H. G., and Gudmundsson, G. H. (1995) *Proc. Natl. Acad. Sci. U.S.A. 92*, 195–9.
28. Wieprecht, T., Apostolov, O., Beyermann, M., and Seelig, J. (1999) *J. Mol. Biol. 294*, 785–94.
29. Bals, R., Weiner, D. J., Meegalla, R. L., and Wilson, J. M. (1999) *J. Clin. Invest. 103*, 1113–7.
30. Marsh, D. (1990) *CRC Handbook of Lipid Bilayers*, CRC Press, Ann Arbor, MI.
31. Whiles, J. A., Brasseur, R., Glover, K. J., Melacini, G., Komives, E. A., and Vold, R. R. (2001) *Biophys. J. 80*, 280–293.
32. Otten, D., Brown, M. F., and Beyer, K. (2000) *J. Phys. Chem. B 104*, 12119–12129.
33. Oldfield, E., Meadows, M., Rice, D., and Jacobs, R. (1978) *Biochemistry 17*, 2727–2740.
34. Koenig, B. W., Ferretti, J. A., and Gawrisch, K. (1999) *Biochemistry 38*, 6327–6334.
35. Hori, Y., Demura, M., Niidome, T., Aoyagi, H., and Asakura, T. (1999) *FEBS Lett. 455*, 228–32.
36. Naito, A., Nagao, T., Norisada, K., Mizuno, T., Tuzi, S., and Saito, H. (2000) *Biophys. J. 78*, 2405–2417.
37. Prenner, E. J., Lewis, R., Kondejewski, L. H., Hodges, R. S., and McElhaney, R. N. (1999) *Biochim. Biophys. Acta 1417*, 211–223.
38. Trouard, T. P., Nevzorov, A. A., Alam, T. M., Job, C., Zajicek, J., and Brown, M. F. (1999) *J. Chem. Phys. 110*, 8802–8818.
39. Lohner, K., Staudegger, E., Prenner, E. J., Lewis, R. N. A. H., Kriechbaum, M., Degovics, G., and McElhaney, R. N. (1999) *Biochemistry 38*, 16514–16528.
40. Hallock, K. J., Wildman, K. H., Lee, D. K., and Ramamoorthy, A. (2002) *Biophys. J. 82*, 2499–2503.
41. Lee, D. K., and Ramamoorthy, A. (1998) *J. Magn. Reson. 133*, 204–206.
42. Lee, D. K., Santos, J. S., and Ramamoorthy, A. (1999) *Chem. Phys. Lett. 309*, 209–214.
43. Lee, D. K., Santos, J. S., and Ramamoorthy, A. (1999) *J. Phys. Chem. B 103*, 8383–8390.
44. Wishart, D. S., and Sykes, B. D. (1994) *Methods Enzymol. 239*, 363–392.
45. Wishart, D. S., Sykes, B. D., and Richards, F. M. (1991) *J. Mol. Biol. 222*, 311–333.
46. Saito, H. (1986) *Magn. Reson. Chem. 24*, 835–852.
47. Henzler Wildman, K. A., Lee, D. K., and Ramamoorthy, A. (2002) *Biopolymers 64*, 246–254.
48. Lee, D. K., and Ramamoorthy, A. (1999) *J. Phys. Chem. B 103*, 271–275.
49. Shoji, A., Ando, S., Kuroki, S., Ando, I., and Webb, G. A. (1993) *Ann. Rep. NMR Spectrosc. 26*, 55–98.
50. Hallock, K. J., Lee, D. K., Omnaas, J., Mossberg, H. I., and Ramamoorthy, A. (2002) *Biophys. J. 83*, 1004–1013.
51. Yamaguchi, S., Huster, D., Waring, A., Lehrer, R. I., Kearney, W., Tack, B. F., and Hong, M. (2001) *Biophys. J. 81*, 2203–2214.
52. El Jastimi, R., Edwards, K., and Lafleur, M. (1999) *Biophys. J. 77*, 842–852.
53. Yamaguchi, S., Hong, T., Waring, A., Lehrer, R. I., and Hong, M. (2002) *Biochemistry 41*, 9852–9862.
54. Matsuzaki, K. (1998) *Biochim. Biophys. Acta 1376*, 391–400.
55. Hallock, K. J., Lee, D. K., and Ramamoorthy, A. (2003) *Biophys. J.*, in press.